Experiments in Fluids 14, 246–256 (1993)

Experiments in Fluids

Flow instabilities during annular displacement of one non-Newtonian fluid by another

M. A. Tehrani, S. H. Bittleston and **P. J. G. Long**

Schlumberger Cambridge Research, Madingley Road, Cambridge CB3 0EL

Abstract. This paper describes an experimental setup for axial laminar flow of liquids in the annulus between two eccentered cylinders. The design uses a conductivity method for measuring peak axial velocities around the annulus, and for the determination of displacement efficiency when displacing one fluid by another (displacement efficiency being defined as the ratio of volume of displaced fluid removed from the annulus, to the volume of the annulus, after a given number of annular volumes have been pumped). In an eccentric annulus, lower axial velocity in the narrow side produces "channeling" of the displacing fluid in the wide side and reduces the displacement efficiency. A positive density contrast between the two fluids can increase the efficiency by promoting azimuthal flow of the (denser) displacing fluid towards the narrow side. In this paper we report that gravity driven azimuthal flow is prone to severe instabilities which accelerate the displacement process but may leave behind an immobile strip of the displaced fluid in the narrow side.

List of symbols

C_m		mean tracer concentration in exit stream
C_0		tracer concentration in displacing fluid
d	m	distance between centres of inner and outer pipes
E		circulation or displacement efficiency
e		non-dimensional eccentricity $[=d/(R_0-R_i)]$
g	$m\,s^{-2}$	gravitational acceleration
h	m	typical annular gap $(=R_o-R_i)$
k	Pa s^n	consistency index in Herschel-Bulkley equation
L	m	hydrostatic head between wide and narrow sides of annulus
n		flow behaviour index in Herschel-Bulkley equation
p	Pa	pressure
Q	$m^3\,s^{-1}$	volume flow rate
R_i	m	inner radius of annulus
R_0	m	outer radius of annulus
r	m	radial distance in annulus
T	s	time
T_b	s	breakthrough time
V	m^3	volume of annulus
w	$m\,s^{-1}$	axial velocity
w_{max}	$m\,s^{-1}$	peak axial velocity
$\bar{w}$	$m\,s^{-1}$	mean flow velocity
z	m	length in direction of flow
$\dot{\gamma}$	s^{-1}	shear rate
θ		angular position around annulus
μ	Pa s	shear viscosity
ϱ	$Kg\,m^{-3}$	fluid density
τ	Pa	shear stress
τ_y	Pa	Herschel-Bulkley yield-stress
ϕ		angle of deviation from vertical

Superscript

* denotes non-dimensionalized quantities such as time, etc.

Subscript

S specifies value of variable at position S along the annulus

1 Introduction

Non-Newtonian fluid flow in eccentric annuli is encountered routinely in the drilling of oil/gas wells and is of particular interest in process industries such as polymer extrusion. The effect of eccentricity is to produce flow velocities in the narrow side considerably lower than those in the wide side of the annulus. In annular flows involving displacement of one fluid by another, this can lead to "channeling" of the displacing fluid (Fluid 2) in the wide side, leaving behind a layer of the fluid to be displaced (Fluid 1) in the narrow side. An example of this is in the cementing of oil/gas wells where the drilling fluid, which initially fills the annulus between the steel casing and the wellbore, is displaced by cement. Good bonding between casing/cement and cement/formation is essential for hydraulic isolation of the well. In addition to eccentricity, displacement efficiency is dependent on the flow regime, fluid properties and deviation of the annulus from vertical.

The technical literature contains many reports of experimental investigation of this type of flow. McLean et al. (1967) performed a qualitative study of the flow by observing the displacement through a transparent wall and measuring externally the angle encompassing the immobile fluid at various positions along an eccentric annulus. Others [e.g. Haut and Crook (1979), Clark and Carter (1973) and Lockyear and Hibbert (1988)] used pilot-scale test rigs to displace drilling fluid with cement. After allowing time for cement to set, the annulus was cut into sections and the displacement efficiency was determined from the areas of cement, casing and borehole. Zuiderwijk (1974) used a radioactive tracer to

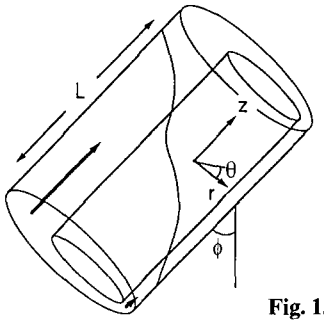

Fig. 1. Driving force for azimuthal flow

measure the drilling fluid left behind by cement along the annulus. For obvious safety and environmental reasons this method has not been widely used.

The above methods have been useful in providing guidelines for specific cementing operations in the field, but are not suitable for detailed studies of fluid flow in eccentric annuli. In this paper we describe a test rig for the laminar flow of model fluids in an annulus, which is capable of producing accurate experimental data for studying the effects of various parameters on displacement. The design offers variable eccentricity and inclination and uses a conductivity method for measuring the overall displacement efficiency and the peak velocity of the interface around the annulus. Lockyear et al. (1989) used conductivity probes to observe the behaviour of the interface between two model fluids and to measure a value for the interfacial velocity. Recently, Beirute et al. (1991) reported use of resistivity probes for estimating the circulatable volume in a pilot-scale annulus containing gelled mud. But, to our knowledge the technique has not been used for direct determination of displacement efficiency in annular flow.

A positive density difference between Fluids 2 and 1 (i.e. $\varrho_2 - \varrho_1 > 0$) is known to improve the displacement efficiency [e.g. see Martin et al. (1978), Haut et al. (1978) and Lockyear et al. (1989)]. Our observations suggest that the mechanism by which density difference operates is in the creation of azimuthal flow of the denser displacing fluid from the wide side to the narrow side of the annulus which improves displacement of Fluid 1 from the narrow side. The driving force for this flow is the hydrostatic pressure imbalance $\Delta\varrho g L \cos\phi$, as shown in Fig. 1. To our knowledge, there are no reports in the literature of instabilities in this type of flow. However, our flow visualizations show evidence of strong azimuthal flow instabilities which accelerate displacement, but are likely to leave behind a thin strip of Fluid 1 in the narrow side. We describe the nature of these instabilities and discuss the mechanism responsible for their occurrence.

2 Experimental methods

This section describes the design of the test rig, the experimental method and test conditions. The method is based on the measurement of variations in electrical conductivity of the test fluid, due to the presence of a tracer (NaCl) in the displacing fluid.

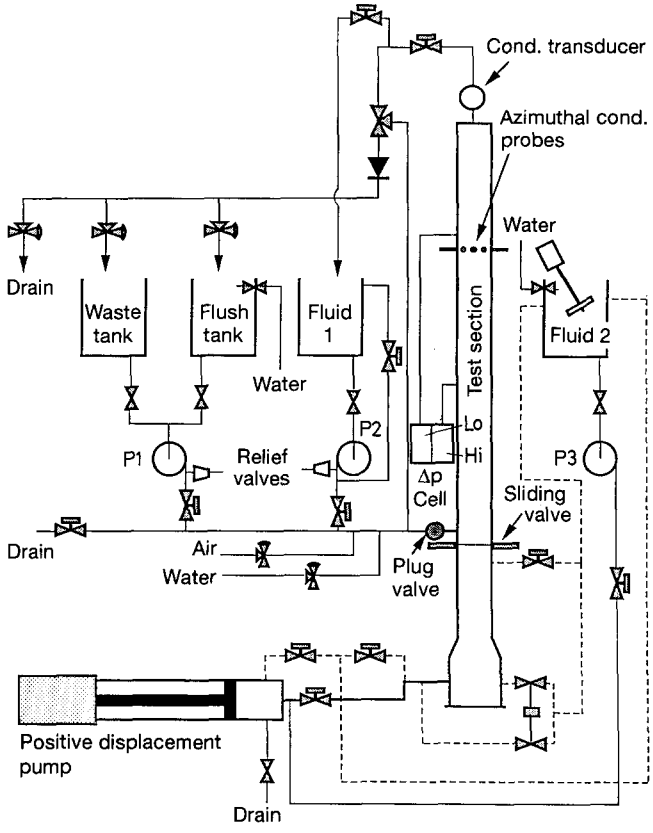

Fig. 2. Schematic of the annular displacement test rig

2.1 Test rig

The layout of the test rig is illustrated in Fig. 2 and a schematic of the test section is shown in Fig. 3. The test section is formed by two cylindrical tubes, one inside the other. The inner tube, or centre-body, has an OD of 4 cm, while the ID of the outer tube is 5 cm, creating a concentric clearance of 5 mm. The centre-body is of stainless steel and functions as a common ground terminal for the conductivity sensors located at position S in Fig. 3. The outer wall is made up of four glass tubes connected by Perspex sleeves.

The annular test section comprises two parts; the displacement volume with a total length of 3 m, preceded by the flow development section. The latter consists of a plenum chamber and a honeycomb flow straightener. The two parts of the annulus can be isolated by a sliding valve which was designed in house. The valve consists of two 0.25 mm thick stainlees steel plates which, in their innermost position, clamp around the centre-body and isolate the test section from the flow development section. The sliding valve is operated by two pneumatic actuators and its operating speed can be altered by adjusting the air pressure.

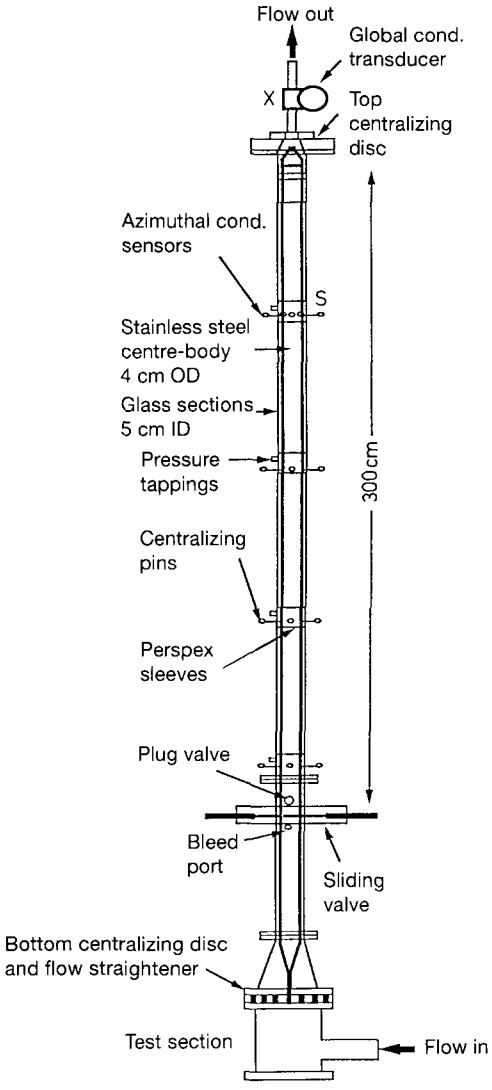

Fig. 3. Schematic diagram of the test section

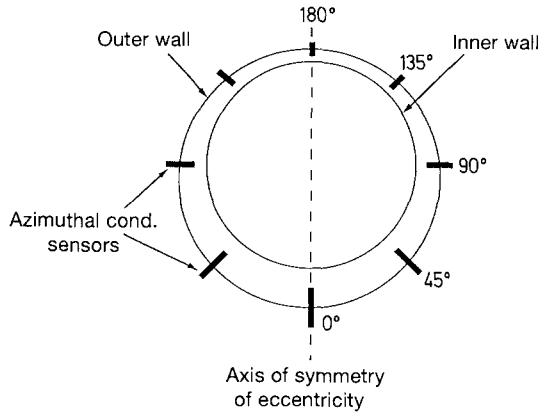

Fig. 4. Arrangement of the azimuthal conductivity probes around an eccentric annulus

Eccentricity can be varied from a concentric to a fully eccentric annulus (where the centre-body and the outer wall are in contact). Alterations to eccentricity are made by means of adjusting screws located in two centralizing mechanisms which support the centre-body. The desired eccentricity is maintained along the test section by five sets of four centralizing pins located at 90° intervals around the annulus. Eccentricity is symmetrical about the axis passing through the wide and narrow sides of the annulus (0° and 180°, respectively).

Conductivity measurements are made at two measuring stations. For the fluid in the test section we use a set of eight conductivity probes at position S (see Fig. 3), while for the exit stream we employ a conductivity transducer at X. The azimuthally positioned conductivity probes, illustrated in Fig. 4, are for the measurement of peak axial velocities around the annulus. The probes are made of 2 mm diameter stainless steel pins welded onto 6 mm diameter adjusting screws. These are inserted into the annulus through threaded bushes fitted inside tapped holes in the outer wall. The radial position of the tip of each probe in the annulus can be adjusted by turning the screw in the bush.

The annular geometry is sensitive to departure of the inner and outer cylinders from perfectly circular cross sections. In our experiments, the maximum variations in the diameters of the two tubes were +0.05 mm for the centre-body and +0.02 mm for the outer wall. Such variations had a very small effect on the velocity distribution around the annulus. We confirmed this by measuring the nonuniformity of the interface around a concentric annulus from breakthrough times (see §2.2) at position S in Fig. 3. We found a maximum variation of less than 1.0% in the height of the interface.

The conductivity transducer (Flow Line Cell Model 2241-604 Transducer, Kent Industrial Measurements) is situated a short distance downstream of the test section and measures the fully-mixed conductivity of the exit fluid. A static mixer, packed with a nylon mesh, is located ahead of the transducer to ensure good mixing in the exit stream. The transducer produces a conductivity trace from which displacement efficiency is calculated.

Displacement is effected by a especially designed piston-type positive displacement (PD) pump. The stainless steel cylinder has an ID of 15 cm and a total capacity of 20 litres. The piston is driven by a servo-controlled ball screw which can provide the necessary acceleration at high pump rates, as well as good precision at low rates. The PD pump can operate in both manual and auto modes. The pumped volume and flow rate are controlled by feed back of position and speed (of the piston) from an optical encoder mounted on the shaft of the ball screw. The pump can produce flow rates in the range 0.01 to 1.5 litre/s, with a tolerance of ±1% of specific flow rate. The design precision for volume control is better than $\pm 0.20\ \text{cm}^3$.

Frictional pressure losses can be measured via 2 mm holes tapped into the test section at positions indicated in Fig. 3. A suitable differential pressure transducer is needed

for this purpose. In our test rig we have installed a Honeywell Model 41105, calibrated to produce a signal of 4–20 mA in the range 0–1400 mm water. The accuracy of the device is ±0.25% of the full scale. The test section can be inclined to any angle from 0° to 90° to the vertical.

Each displacement test involves a sequence of procedures, including:

- washing, draining and drying of the annular space,
- filling of the annular space with Fluid 1,
- filling of the positive displacement feed pump with Fluid 2,
- flushing of all pipes upstream of sliding valve with Fluid 2.

Balancing of pressures on the two sides of the sliding plates is a crucial factor in obtaining a smooth interface before the start of a test.

The test rig can be operated in either "manual" or "auto" mode. Displacement tests are normally conducted in the "auto" mode. Computer control is by a main test computer which communicates via an RS422 serial link with the microprocessor controlling the positive displacement pump. The main test computer controls the inclination of the test section and is interfaced with the conductivity sensors for displacement data acquisition. The controlling software is in BBC BASIC with CONTROL BASIC extensions.

2.2 *Experimental procedure*

To perform a displacement test, the upper and lower parts of the test section are first filled with Fluids 1 and 2, respectively. The two fluids are kept apart by the sliding valve. At time zero the sliding valve opens and the fluids are brought into contact across a flat interface in the r,θ plane. A piston-type positive displacement pump then injects a known volume of the displacing fluid into the test section at controlled flow rate. The interface between the two fluids moves forward along the test section as displacement of Fluid 1 takes place. Simultaneously, data acquisition begins which consists of the time, volume (of Fluid 2) pumped and the conductivity signals from different sensors.

The azimuthal conductivity probes at S detect the arrival of the interface by the discontinuity in the tracer (salt) concentration. From the conductivity traces produced by the probes, the times of first arrival of Fluid 2 at various positions around the annulus are measured, i.e. breakthrough time $T_{b,S}(\theta)$. The peak velocities are then calculated from

$$\frac{w_{\max}(\theta)}{\bar{w}} = \frac{1}{T^*_{b,S}(\theta)} = \frac{V_S}{Q\,T_{b,S}(\theta)}, \tag{1}$$

where $T^*_{b,S}$ is the non-dimensional breakthrough time at position S. The dimensionless time T^* is also the number of annular volumes (of Fluid 2) pumped. Figure 5 shows typical conductivity traces produced by the azimuthal probes in an annulus with 50% eccentricity. It can be seen that the

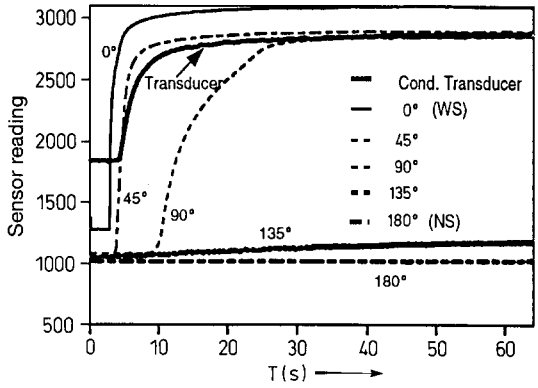

Fig. 5. Typical conductivity traces (raw data) for displacement in a vertical eccentric annulus with 50% eccentricity, Re = 220

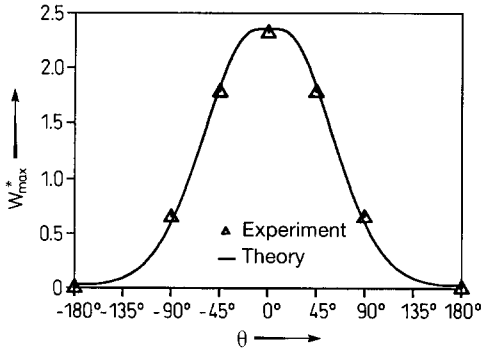

Fig. 6. Variation of peak axial velocity around an eccentric annulus, $e = 0.5$, Re = 220

arrival of the interface at S occurs first in the wide side and then gradually at other positions around the annulus. In particular, we note that there is little or no axial flow in the narrow side of the annulus. Figure 6 is an example of variation of the peak velocities around the annulus. The solid line is the predictions of a theoretical solution referred to in §2.4.

Displacement efficiency is defined as the volume fraction of Fluid 2 in the annulus. This is equivalent to the volume of Fluid 1 removed from the annulus divided by the annular volume. Thus, up to the breakthrough time, efficiency is proportional to flow rate,

$$E(T) = \frac{Q\,T}{V} = T^* \quad T \le T_b\,. \tag{2}$$

Here, T_b is the time of first arrival of the interface at the top of the annulus. This is obtained from the trace produced by the conductivity transducer, after allowing for the additional distance to position X. After breakthrough, efficiency continues to increase, albeit at a reducing rate. Referring to Fig. 7, we can write for the fluid at the top of the annulus,

$$\frac{C_m(T)}{C_0} = \frac{2\int_0^{\pi}\int_{r_1(\theta,T)}^{r_2(\theta,T)} r\,w(r,\theta)\,\mathrm{d}r\,\mathrm{d}\theta}{Q}, \tag{3}$$

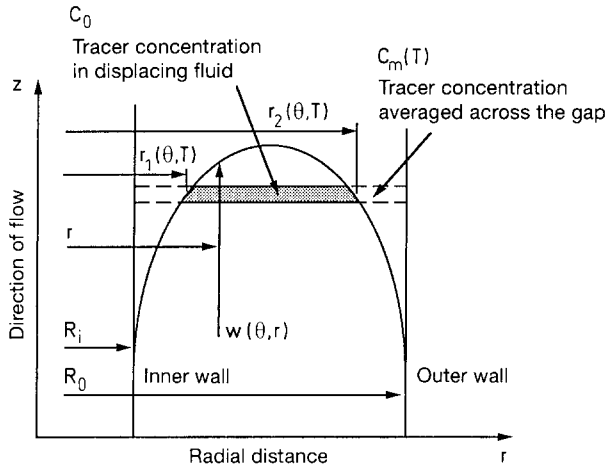

Fig. 7. Arrival of interface at top of annulus

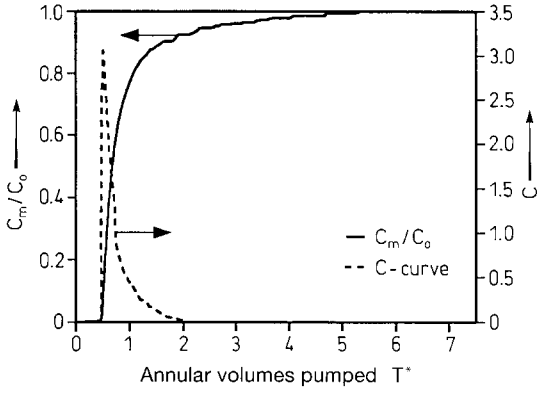

Fig. 8. Normalized trace (C_m/C_0) produced by the conductivity transducer, and residence time distribution (C-curve) for the exit stream. The curves correspond to the data of Fig. 5

where r is the radial position across the annular gap and $w(r, \theta)$ is the axial velocity. Note that the limits of the second integral, which are dependent on both azimuthal position θ and time T, are located on the interface at the exit of the test section. Equation (3) describes the volume fraction of Fluid 2 in the exit stream in terms of the time-dependent non-dimensional mean concentration of the tracer in the fluid. The rate of removal of Fluid 1 from the annulus is now given by $[1-C_m(T)/C_0]Q$. Therefore, displacement efficiency at any time after breakthrough is described by,

$$E(T)=\frac{Q\,T_b+\int_{T_b}^{T}[1-C_m(T)/C_0]\,Q\,\mathrm{d}T}{V},\quad T_b<T. \tag{4}$$

In terms of the non-dimensional time T^*, equation (4) becomes,

$$E(T^*)=T^*-\int_{T_b^*}^{T^*}\frac{C_m(T^*)}{C_0}\,\mathrm{d}T^*. \tag{5}$$

In our experiments, a small tracer loading (C_0) ensures that the relationship between conductivity and tracer concentration remains linear during a displacement test. As a result, C_m/C_0 can be obtained from the normalized form of the conductivity trace produced by the transducer at X (see Fig. 5). Referring to the plot of the normalized trace in Fig. 8, it can be seen that the first term in Eq. (5), T^*, is the number of annular volumes of Fluid 2 pumped. The second term, the area under the C_m/C_0 curve, is the annular volumes of Fluid 2 that has left the annulus since breakthrough. The difference between the two terms, i.e. the area above the curve, is the volume fraction of the displacing fluid in the annulus (or the volume fraction of Fluid 1 removed from the annulus). Thus, displacement efficiency is equal to the area above the C_m/C_0 curve and has an upper limit of unity.

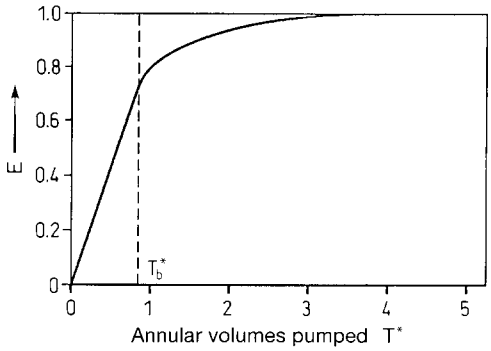

Fig. 9. Variation of overall efficiency with time for displacement in a concentric annulus, Re = 30

The normalized trace is also the cumulative age distribution of the tracer in the exit stream. An alternative approach, therefore, is to consider the slope of the C_m/C_0 curve, which is the residence time distribution of the tracer in the exit stream, i.e. the $\boldsymbol{C}$-curve [see, for example, Levenspiel (1972)]. The mean of the $\boldsymbol{C}$-curve, in the limits of $\boldsymbol{C}(T^*)=0$ for $T^*\le T_b^*$ and $\boldsymbol{C}(T^*)=0$ when $T^*=T_f^*$, is given by:

$$T^*_{\mathrm{mean}}=\frac{\int_{T_b^*}^{T_f^*}T^*\,\boldsymbol{C}(T^*)\,\mathrm{d}T^*}{\int_{T_b^*}^{T_f^*}\boldsymbol{C}(T^*)\,\mathrm{d}T^*}, \tag{6}$$

where $\int_{T_b^*}^{T_f^*}\boldsymbol{C}(T^*)\,\mathrm{d}T^*$, area under the $\boldsymbol{C}$-curve, is unity. Replacing for $\boldsymbol{C}(T^*)$ from

$$\boldsymbol{C}(T^*)=\frac{\mathrm{d}[C_m(T^*)/C_0]}{\mathrm{d}T^*} \tag{7}$$

and integrating by parts, equation (6) becomes,

$$T^*_{\mathrm{mean}}=E(T_f^*)=T_f^*-\int_{T_b^*}^{T_f^*}\frac{C_m(T^*)}{C_0}\,\mathrm{d}T^*. \tag{8}$$

Therefore, displacement efficiency after a sufficiently long time T_f^*, i.e. when $C_m(T^*)/C_0=1$, is equal to the mean of the residence time distribution of the tracer in the outflow.

Figure 9 shows the efficiency curve for displacement in a concentric annulus. The bulk of the displacement occurs

before breakthrough. After breakthrough the rate of displacement decreases gradually as most of the displacing fluid pumped into the test section leaves the annulus. Figure 9 indicates that, even in a concentric annulus, more than three annular volumes of Fluid 2 are required in order to achieve 99% displacement. We never completely remove the original fluid.

2.3 Dynamic similarity

To achieve flow conditions similar to those encountered in the cementing of oil wells, we used dynamic similarity to scale the experiments. Geometric similarity was provided by choosing a radius ratio for the annulus comparable to those in the field, i.e. $R_i/R_0 = 0.8$. The aspect ratio of the annulus (length to width ratio of 600), although smaller than that of a typical annulus in cementing, was found to be well in excess of that required to produce a fully developed laminar velocity profile. We also matched the experimental values of the dimensionless parameters governing the flow with those in the field. These parameters, which arise from the formulation of the problem for displacements involving two generalized Newtonian fluids, i.e. non-Newtonian fluids which may exhibit a yield stress but no thixotropy or elasticity, include a Reynolds number for each fluid i ($i=1$ for Fluid 1, $i=2$ for Fluid 2),

$$\mathrm{Re}_i = \frac{2\varrho_i \bar{w} h}{\mu_i}, \tag{9}$$

and a buoyancy number defined by:

$$\mathrm{Bu} = \frac{\Delta\varrho g h^2}{\bar{w}\mu_2}, \tag{10}$$

which is the ratio of buoyancy to viscous forces. Note that $\mathrm{Bu}=0$ for the flow of a single fluid in the annulus. Reynolds numbers were in the range 0.8 to 260 and the buoyancy numbers varied from 0 to 13.

2.4 Test conditions

The design of the test rig is such that, with suitable choice of displacement fluids, it allows both quantitative and qualitative studies of (non-Newtonian) fluid displacement in an annulus. To model the oilfield fluids, in our experiments we used solutions of a commercial *xanthan* gum Idvis (supplied by International Drilling Fluids) as the base fluid. A weighting agent was added where required to produce a density difference between Fluids 1 and 2. The weighting agent was precipitated barium sulphate (Blanc Fixe) manufactured by Rhône-Poulenc Chemicals, with a density of 4200 Kg/m^3 and mean particle size 2 μm. A Baroid 286 Variable Speed Rheometer measured the rheology of the solutions at twelve shear rates in the range 5.11 – 1022 s^{-1}. The fluid exhibited a concentration-dependent apparent yield-stress and its rheology was found to be well represented by the Herschel-Bulkley (1926) model,

$$\tau = \tau_y + k\dot{\gamma}^n. \tag{11}$$

Typical values of the rheological parameters were: $\tau_y = 1.22$ Pa, $k = 0.197$ Pa s^n and $n = 0.505$. We performed displacement tests using several density differences (0–20%), flow rates (0.01–0.30 L/s) and eccentricities (0–100%).

3 Results and discussion

In this section, we report quantitative results of experiments involving flow of a single fluid. These were used to examine the performance of the test rig for non-Newtonian displacement. We also discuss secondary flow instabilities observed in flow visualizations of displacement in the presence of a positive density difference.

3.1 Performance tests

The experimental rig had previously been used by Long (1991) in his study of Newtonian fluid displacement in annuli. We examined the performance of the test rig for non-Newtonian displacements by conducting a series of experiments in which the two fluids were identical except for a small concentration of the tracer in Fluid 2 for conductivity measurements. These are referred to as single fluid circulation tests. An example of this type of flow is in the circulation phase preceding a cementing operation where the gelled drilling fluid in the annulus is mobilized by circulation around the wellbore. The magnitude of the peak axial velocity $w_{\max}(\theta)$ is a good indication of local mobility of the fluid around the annulus, while E provides an accurate measure of the overall circulation efficiency.

We compared the results of the (single fluid) circulation tests with predictions of a theoretical solution for the steady unidirectional flow of a yield-power law fluid in an eccentric annulus. The solution uses a numerical scheme to solve the governing flow equations. The numerical method is that reported by Walton and Bittleston (1991) for the axial flow of a Bingham plastic in a narrow eccentric annulus, with appropriate modification for a yield-power law fluid.

Figure 10 compares theory with experiment for the non-dimensional peak velocities, $W^*_{\max} = w_{\max}/\bar{w}$. In a concentric annulus, axial velocity profile is constant around the annulus, with $W^*_{\max} = 1.18$. This is considerably lower than that for Newtonian flow in the same geometry, where analytical solution suggests $W^*_{\max} = 1.50$. In an eccentric annulus, restriction of flow in the narrow side results in higher velocities in the wide side. Peak velocity in the wide side has its highest values with ~50% eccentricity. In Fig. 10, for $e = 0.5$, $W^*_{\max}$ is 90% higher than in a concentric annulus. In annuli with 50% or more eccentricity, the fluid can become effectively immobile in the narrow side.

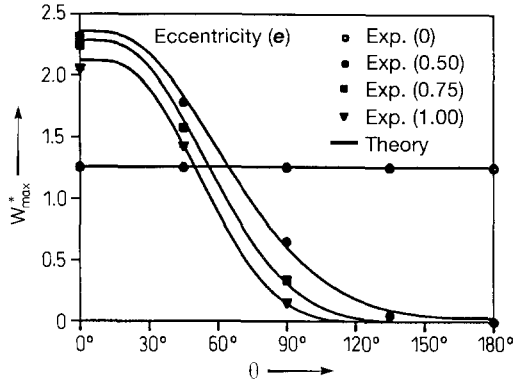

Fig. 10. Variation of peak axial velocity around the annulus for the flow of a single yield-power law fluid, Re = 220

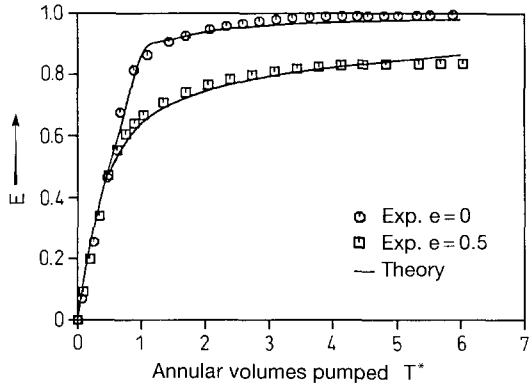

Fig. 11. Circulation efficiency in eccentric annuli for a yield-power law fluid, Re = 220

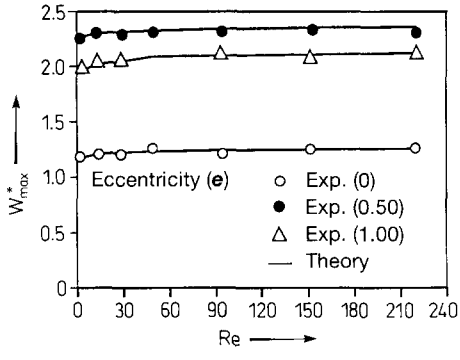

Fig. 12. Variation of peak axial velocity (at $\theta = 0$) with Reynolds number for the flow of a single fluid in the annulus

Figure 11 illustrates the effect of eccentricity on circulation efficiency. Up to the breakthrough time, efficiency increases linearly with hole volumes pumped. Displacement becomes progressively more difficult after breakthrough. We see that in a 50% eccentric annulus, about 20% of the fluid remains uncirculated after six annular volumes have been pumped.

In the laminar region, higher flow rates produce a small increase in the peak axial velocity around the annulus. This

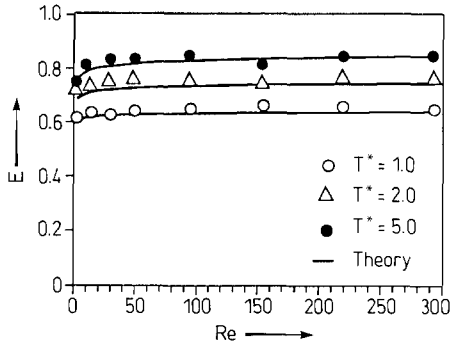

Fig. 13. Effects of Reynolds number and annular volumes pumped on circulation efficiency in an annulus with 50% eccentricity

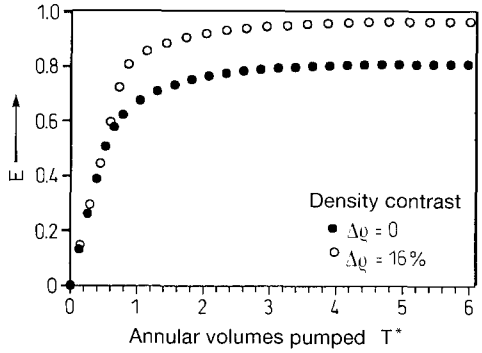

Fig. 14. Effect of density contrast on displacement efficiency in a vertical annulus, Re = 176, $e = 0.5$

is illustrated in Fig. 12 for W^*_{max} (corresponding to $\theta = 0$) vs. Reynolds number at several eccentricities. The solid lines represent theoretical predictions.

The increase in the peak velocity results in a slight improvement in circulation efficiency. Fig. 13 shows the effects of Reynolds number and annular volumes pumped on efficiency, in an annulus with 50% eccentricity. Whereas flow rate has only a small effect on displacement, larger volumes of Fluid 2 can increase the efficiency significantly. However, in oilfield practice the amount of fluid pumped is limited, and optimizations are generally aimed at displacement with one annular volume.

The agreement between experiment and theory is good. For the peak velocities in the wide side of the annulus the difference is 2%, increasing somewhat towards the narrow side. Circulation efficiencies show an average difference of approximately 2%.

3.2 Secondary flow instabilities

A positive density difference between the displacing and displaced fluids can improve the displacement efficiency in an eccentric annulus. An example of this is shown in Fig. 14

where we compare efficiencies for a single fluid circulation ($\Delta\varrho = 0$) and a displacement involving two fluids with similar rheologies but with 16% density difference (Re = 176, $e = 0.5$). The improvement in efficiency after one annular volume is about 16.5%.

In such a geometry, where the displacing fluid has a tendency to channel through the wide side, density difference produces a hydrostatic pressure imbalance between the wide and narrow sides. This imbalance induces a secondary gravity-driven azimuthal current from the wide side to the narrow side of the annulus. Regardless of eccentricity, density difference also induces secondary radial flows across the annular gap. This is due to a hydrostatic pressure imbalance between the central part of the annulus and regions near the walls. The relative strengths of the azimuthal and radial currents depends on eccentricity and the rheology of the fluids.

The interface between two miscible fluids with similar rheologies, but with different densities, is stable so long as the denser fluid lies below the interface, and the interface is not near vertical. When flow conditions are such that the interface becomes close to vertical, small perturbations in the flow field may trigger gravity driven interfacial instabilities. We observed such instabilities when we performed flow visualizations of displacement in a vertical eccentric annulus in the presence of a positive density difference. In these experiments the partially transparent Fluid 1 was coloured with a water soluble red dye, while the displacing fluid was completely opaque, with white colour due to the weighting agent. The annulus was viewed from the narrow side at an angle perpendicular to the direction of flow. We observed displacement over a range of flow rates and density differences.

We found that under certain conditions, significant azimuthal instablities occur which appear to accelerate displacement in the narrow side of annulus. To our knowledge, there are no reports in the literature of instabilities in such gravity induced secondary flows. Our observations show that the intensity of azimuthal instabilities is related to density difference and flow rate. Larger values of $\Delta\varrho$ promote instabilities while higher flow rates have the opposite effect. This suggests that the relative strength of azimuthal to axial flow is an important factor in the occurrence of instabilities. Flow conditions which increase the relative strength of secondary azimuthal currents with respect to axial flow may trigger or intensify azimuthal instabilities. In this respect, higher eccentricities may also favour the occurrence of instabilities.

Noting the driving force for azimuthal flow in a vertical annulus by $\Delta\varrho g L$, and for axial flow by $\frac{1}{2}\varrho_2 \bar{w}^2$ (based on the displacing fluid), the relative strength of azimuthal to axial flow is given by $2\Delta\varrho g L/\varrho_2 \bar{w}^2$. This is a ratio of static to dynamic pressures and is similar to the ratio of buoyancy number (defined as $\mathrm{Bu} = \Delta\varrho g h^2/\mu_2 \bar{w}$) to Reynolds number ($\mathrm{Re} = 2\varrho_2 \bar{w} h/\mu_2$) of the flow. An increase in this ratio would enhance azimuthal flow and may trigger instabilities.

One must not overlook the role of fluid rheology in this process. In our flow visualizations, Fluids 1 and 2 had similar rheologies, i.e. similar shear stresses at like shear rates. In such instances, the condition for the azimuthal currents to mobilize the fluid in the narrow side is governed by the hydrostatic head L, as well as the dimensions of the annulus. To illustrate this point, we consider the simplified case of displacement in an eccentric annulus with mean radius r_m and average gap size h_m. The momentum equation for steady azimuthal flow then reduces to a balance between the pressure and viscous forces [see Bird et al. (1987)],

$$0 = -\Delta p\, h_m + 2\pi r_m \tau_w, \tag{12}$$

in which Δp is the pressure force driving the azimuthal flow, given by $\Delta\varrho g L$, and τ_w is the wall shear stress. For the fluid to flow, shear stress at the wall must exceed the yield stress. Therefore, the condition for flow is

$$\Delta\varrho g L \frac{h_m}{2\pi r_m} > \tau_y \tag{13}$$

The above equation sets the minimum required value for the hydrostatic head L, and is expected to be easily satisfied in an eccentric annulus. For typical oilfield data, e.g. $\tau_y = 10$ Pa, $\Delta\varrho = 250$ Kg/m^3, $R_i = 0.089$ m and $R_0 = 0.111$ m, the minimum required value for L is about 0.11 m.

The above example serves to illustrate that for fluids with a yield stress, a relatively small hydrostatic head is sufficient to mobilize the fluid in the narrow side. However, for instabilities to occur, L must be such that the interface assumes a near vertical profile between the wide and narrow sides of the annulus. This value can be determined from properly scaled experiments. In our experiments with $e = 0.5$, the hydrostatic head producing the instabilities was of order 1–2 m.

We categorize the mechanism for displacement in the narrow side according to whether or not azimuthal instabilities occur in the flow:

1. In stable flow, or when the instabilities appear only as wavy motion of the interface, Fluid 2 flows towards the narrow side by means of the azimuthal velocity component induced by the pressure imbalance between the wide and narrow sides, e.g. points **a** and **b** in Fig. 15. Within Fluid 2, in the vicinity of the line of symmetry in the narrowest part, the azimuthal component is transformed into axial velocity, with the consequent result of Fluid 2 displacing Fluid 1 in the narrow part of the annulus. Continuity of the velocity field dictates that, within Fluid 1, the velocity vectors near the interface point in the direction of the main flow and slightly towards the wide side (i.e. away from the line of symmetry), setting up a weak reverse azimuthal flow, as depicted in Fig. 15.

When azimuthal flow is strong but stable, i.e. large $\Delta\varrho$ and relatively high flow rate, displacement by azimuthal currents takes place more or less simultaneously along most of the axial spread of the interface, i.e. L. Consequently, the driving force for azimuthal flow decreases rapidly as the interface

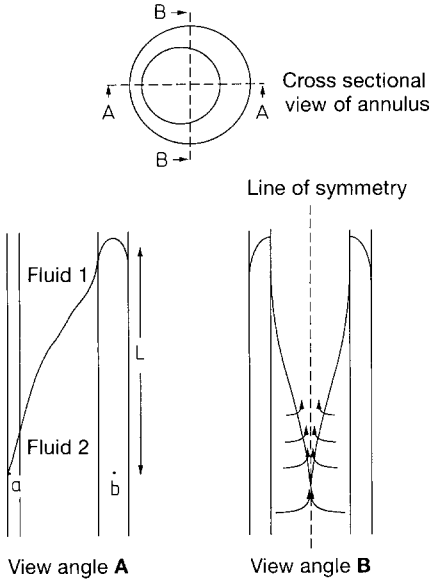

Fig. 15. Hydrostatic pressure imbalance resulting in secondary azimuthal flow in an eccentric annulus. Arrows show direction of velocity vectors (mean across the annular gap) near the narrow side

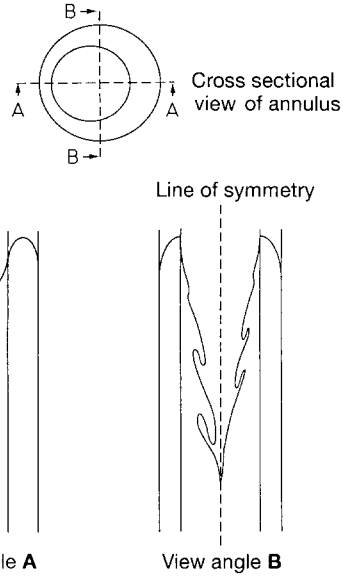

Fig. 17. Schematic diagram showing azimuthal instabilities

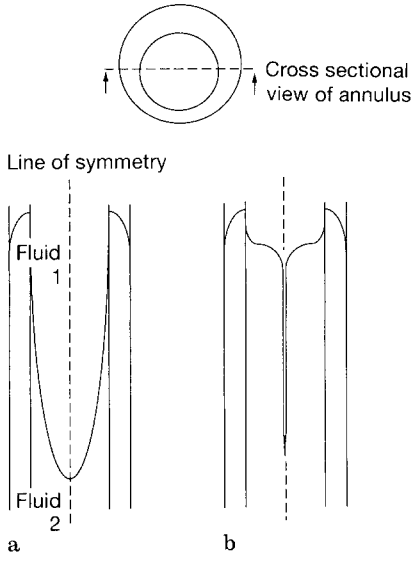

Fig. 16 a and b. Effect of (stable) azimuthal flow on displacement, **a** early stage in displacement, **b** advanced stage in displacement with a narrow strip of Fluid 1 left at the line of symmetry

approach the line of symmetry in the narrow side. At this stage, the annulus is filled with the displacing fluid except for a thin strip of Fluid 1 in the narrow side, which becomes very difficult to remove. Fig. 16a shows an early stage in the displacement, while Fig. 16b depicts an advanced stage when the annulus is filled with Fluid 2, except for thin strip of Fluid 1 at the line of symmetry.

2. When $\delta\varrho\, g\, L\frac{h_m}{2\pi r_m} - \tau_y \gg 0$ and the ratio of static of dynamic pressures is relatively large, i.e. low flow rates, the reverse azimuthal flow field set up in Fluid 1 "cuts" into the interface which is advancing towards the narrow side and triggers flow instabilities. Where the instabilities are severe, Fluid 2 flows towards the narrow side through formation of fingers branching away from the main axial flow. Since the motion of the fingers is towards the narrow side, they move at a lower axial velocity than the main body of Fluid 2 and appear to be falling away at the interface. As the fingers cascade towards the narrow side, streams of Fluid 1 become trapped between the fingers and the main body of Fluid 2. These streams are directed towards the wider part of the annulus and are carried away by the main body of Fluid 2. This mechanism is illustrated in the schematic diagram of Fig. 17. In situations of high azimuthal instability, the falling fingers accelerate displacement in the narrow side. However, in most cases a thin wavy strip of Fluid 1 is left behind in the narrow side, as shown in the photograph of Fig. 18. In addition, small pockets of Fluid 1 may become trapped in the narrow side where they are likely to remain indefinitely. Figs. 19a and b show photographs of such instabilities at two levels of intensity.

When the two fluids have different rheologies, azimuthal flow has to overcome the yield stress of the more viscous fluid in the narrow side in order to affect displacement. Where Fluid 1 has a higher yield stress than Fluid 2 and the driving force for azimuthal flow is not sufficient to mobilize Fluid 1, then circulation currents are expected to be set up near the interface in Fluid 2, with little or no contribution to displacement of Fluid 1 in the narrow side.

The scaling by dynamic similarity (see §2.3) suggests that gravity driven instabilities can also occur under field conditions. Furthermore, we note that in normal field practice for laminar displacement, the displacing fluid is both denser and

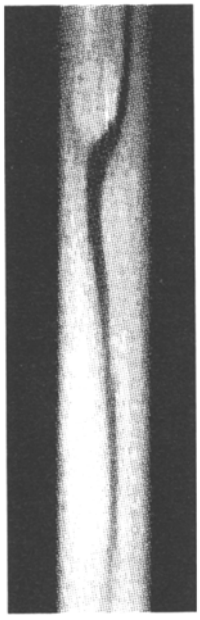

Fig. 18. Azimuthal instabilities leave a wavy strip of Fluid 1 in the narrow side

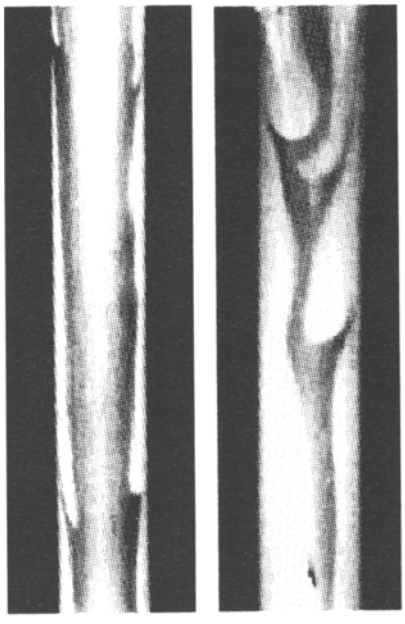

a b

Fig. 19 a and b. Photographs of azimuthal instabilities at **a** low and **b** high levels of intensity

has a higher apparent viscosity than the displaced fluid. Therefore, any interfacial instabilities that may occur as a result of viscous fingering, will be augmented by the density contrast when the interface is near vertical in a highly eccentric annulus.

4 Conclusion

We describe an experimental test rig for the study of fluid displacement in an annulus. The annular test section provides variable eccentricity and inclination. A sliding valve mechanism produces a clean interface between the displaced and displacing fluids at the start of each test. The measurement technique uses conductivity probes to measure peak axial velocities and the overall displacement efficieny. The design is particularly useful for investigation of non-Newtonian flow where problems of nonmobility may exist under certain conditions of geometry, flow and material properties.

The performance of the apparatus was tested successfully by comparing the measured peak velocities and overall efficiencies against theoretical predicitions for the laminar flow of a yield-power law fluid in an annulus. We have given several examples of single fluid circulation and two fluid displacement. The measurements indicate that:

1. Eccentricity has the greatest effect on displacement in an annulus. Minimum efficiency occurs at about 50% eccentricity.
2. Flow rate of the displacing fluid has a small positive effect on displacement in an eccentric annulus.
3. Pumping larger volumes of the displacing fluid increases the displacement efficiency.
4. In displacements in a vertical annulus, a positive density contrast between the displacing and displaced fluids improves the efficiency.

Flow visualizations in an eccentric annulus reveal azimuthal flow instabilities occurring in two-fluid displacements where a positive density difference exists between the two fluid. Such instabilities accelerate the displacement process but leave behind a thin channel of the displaced fluid in the narrow side of the annulus. We suggest that instabilities occur due to a reversal of the azimuthal flow field in the displacing fluid.

Acknowledgements

We thank S. Muller (now at University of California, Berkeley) for her part in the design and construction of the test rig and P. Faupel for providing technical support throughout the project. We also thank I. Sobey (Oxford University, Computing Laboratory) for his valued advice on theoretical aspects of the work.

References

Beirute, R. M.; Sabins, F. L.; Ravi, K. V. 1991: Large-scale experiments show proper hole conditioning: A critical requirement for successful cementing operations. SPE Paper 22774. Presented at the 66th Annual Conference, Dallas, Oct.

Bird, R. B.; Armstrong, R. C.; Hassager, O. 1987: Dynamics of polymeric liquids. Volume 1: Fluid mechanics (second edition). Appendix B. New York: Wiley

Clark, R. C.; Carter, L. G. 1973: Mud displacement with cement slurries. J. Pet. Tech., July 775–783

Haut, R. C.; Collins, R. E.; Graves, W. G. 1978: Applications of a computer simulator to primary cementing. SPE Paper 7588. Presented at the 53rd Annual Conference, Houston, Oct.
Haut, R. C.; Crook, R. J. 1979: Primary cementing: The mud displacement process. SPE Paper 8253. Presented at the 54th Annual Conference, Las Vegas, Sep.
Herschel, W. H.; Bulkley, R. 1926: Konsistenzmessungen von Gummi-Benzollösungen. Kolloid Z. 39, 291–300
Levenspiel, O. 1972: Chemical Reaction Engineering. Chapter 9. New York: Wiley
Lockyear, C. F.; Hibbert, A. P. 1988: A novel approach to primary cementation using a field scale flow loop. SPE Paper 18376. Presented at the European Petroleum Conference. London, Oct.
Lockyear, C. F.; Ryan, D. F.; Gunningham, M. M. 1989: Cement channeling: How to predict and prevent. SPE Paper 19865. Presented at the 64th Annual Conference, San Antonio, Oct.
Long, P. J. G. 1991: Experimental studies of fluid-fluid displacement in annuli. Ph.D. thesis, Cambridge University
Walton, I. C.; Bittleston, S. H. 1991: The axial flow of a Bingham Plastic in a narrow eccentric annulus. J. Fluid Mech. 222, 39
Zuiderwijk, J. J. M. 1974: Mud displacement in primary cementing. SPE Paper 4830. Presented at the European Spring Meeting, Amsterdam, May

Received September 21, 1992

Announcements

5th International Conference Laser Anemometry – Advances and Applications, Koningshof, Veldhoven, The Netherlands, 23rd–27th August 1993

Introduction

International Conferences were held in the UK at the Universities of Manchester, Strathclyde, Swansea and in Cleveland, USA in December 1985, September 1987, September 1989 and in August 1991 respectively. It is now planned to hold the fifth conference in the series at Koningshof, the Netherlands which is situated in the provence of Brabant near Eindhoven. This venue offers a most attractive combined location for the meeting and is easily accessed by road, rail or air.

The meeting will take place from Monday 23rd until Friday 27th August 1993 and will follow the same proven format as in the previous highly successful meetings. All submitted abstracts will be reviewed and papers will be refereed before acceptance. The number of parallel sessions will be minimised. Poster Sessions will be arranged for most recent findings or highly specialised topics.

Papers are sought on every aspect of Laser Anemometry, although those making reference to "Advances in techniques" and "Special applications" will be particularly welcome. The following list is offered for guidance.

Techniques	*Flow-types*
Laser Doppler anemometry	Single-phase fluid mechanics
Two-spot velocimetry	Two-phase flow and particle sizing
Whole field velocimetry	Effects of temperature on flow
Particle image velocimetry	High speed flows
Doppler pictures	Unsteady flows
New optical schemes	Separated flows
Fibre optics	Biomedical flows
Refractive index matching	Combustion and reacting flows
Miniature laser velocimeters	Cavitation
Signal processing	Atmospheric boundary layer flow
Data acquisition, processing, reduction	Rotating and reciprocating machinery
Non standard forms of laser anemometry	
Comparison between codes and experiments	

Note that this list is not meant to be exhaustive and that papers in other subject areas will be considered.

Offers of papers

Authors are invited to submit titles and extended abstracts (500 words minimum plus supporting figures) on topics appropriate to the conference. The abstract should be sent to the Conference Address as soon as possible and certainly not later than 1 October 1992.

Subject to acceptance of this abstract, completed papers having a text of 3,000–5,000 words will be required for refereeing by 15 February 1993. Final acceptance of the paper will depend upon the referees' judgement of the draft mansucript and receipt of the corrected camera-ready proof (incorporating any specified corrections) before 15 May 1993. Here, authors should note that the Proceedings Volumes from the former conferences are on sale from the British Hydromechanics Research Association, Cranfield, and that hard bound volumes from the second conference in Strathclyde and third conference in Swansea have been distributed by Springer-Verlag.

Further notes to authors

In all cases work must be original and should not have been published nor offered for publication elsewhere. Papers must be written and presented in English. Papers accepted for presentation will be available to delegates at the time of the meeting. Authors are expected to present their papers in person and to attend the meeting as delegates.

National representatives are currently being appointed to assist with planning and advertising the conference. Full details will be available in the next announcement.

Invited lectures will be given by acknowledged experts on several topics selected by the Organising Committee. Details of these will be available in the second announcement due for release in July 1992.

Enquiries and all Correspondence should be addressed to: Ms. J. Schellingerhout, L.A. *Conference* 1993, Dr. Ter Braaklaan 1, NL-4002 WN Tiel, The Netherlands, Telephone: +31 3440 1 57 63/ 1 63 84, Fax: +31 3440 2 41 03.